EAN 2020
58th conference on experimental stress analysis

Tensile Tests of 3D Printed PLA and Calibration of an Orthotropic Material Model

HECZKO J.[1,a], KRYSTEK J.[1,b], KOTTNER R.[1,c]

[1]NTIS - New Technologies for the Information Society, Faculty of Applied Sciences, University of West Bohemia, Technicka 8, Pilsen, Czech Republic

[a]jheczko@ntis.zcu.cz, [b]krystek@ntis.zcu.cz, [c]kottner@ntis.zcu.cz

Keywords: 3D printing, PLA, Tensile test, Anisotropic material, Orthotropic material model

Abstract. Tensile tests of a desktop 3D printed polylactic acid (PLA) material are presented. Four different angles of infill orientation were measured, all with the same infill density of 100 %. Poisson's ratios were determined in another set of tests using strain gauges and larger specimens. Calibration of a linear orthotropic material model was performed.

Introduction

Additive manufacturing and 3D printing are nowadays a widely used tool for not only rapid prototyping, but manufacturing of both functional prototypes and final products. Many technologies emerged over the past decades, ranging from stereolithography and fused deposition modelling (FDM) to sintering and jetting methods. Further development of these technologies includes printing from a vast amount of materials (plastic composites, concrete, food [1], biological tissues [2]), continuous fibre reinforcement, non-planar printing or 4D printing [3].

The study of mechanical properties of objects made by additive manufacturing is somewhat lacking this rapid development and the results may even be a little contradictory [4]. These are, however, crucial for ensuring functionality of the printed parts and should be taken into account in the design process. Technical data sheets often provide strength and stiffness of the raw material, but the resulting properties may depend heavily on the technology and setup of the printing process, e.g. (in the case of fused deposition modelling (FDM) technology) nozzle temperature, volume flow ratio, printing speed, part orientation or layer thickness [4-6].

This work focuses on stiffness and strength of PLA printed on a desktop FDM machine, since this is usually a starting point for most 3D printing projects. Moreover, the results, especially testing methods and modelling, may be applicable to the more sophisticated printing technologies and products of industrial machines. Previous works relevant to this particular choice of objectives include the following.

Andrzejewska et al. [7] performed monotonic and fatigue tests of both injection molded and 3D printed PLA. They used two different orientations (±45° and 0/90°) and two different densities (30 % and 90 %) of a rectilinear infill pattern and one type of honeycomb pattern. They found that the usual dogbone shape of specimens (ISO 527) is suitable for both injection molded and FDM/FFF 3D printed material.

Fernandez-Vicente et al. [8] evaluated the effects of infill pattern and its density on ultimate stress, ultimate strength, and Young's modulus ABS for a single orientation of specimens showing that 100 % infill may reach similar properties as the raw material.

Nomani et al. [9] compared different values of layer thickness between 0.2 mm and 0.8 mm, showing that strength and stiffness of ABS increase with decreasing layer thickness.

Pandzic et al. [10] studied the effect of PLA colour on various mechanical properties. The Young's modulus ranges between 2.7 and 3.2 GPa and tensile strength ranges between 30 and 41 MPa.

Verbeeten et al. [11] tested the anisotropy of rate-dependent behaviour of PLA showing that both elastic and viscous properties are anisotropic.

Doungkom and Jiamjiroch [12] compared the impact of specimen orientation with respect to the build plate in the case of PLA and different densities of the honeycomb infill pattern.

Cooling of the printed object has been shown to impact both dimensional quality and mechanical properties. Higher speeds of cooling air led to better accuracy but lower tensile strength, especially if the loading direction is perpendicular to the direction of printing [13]. Lower strength is explained by higher void ratio and lower crystallinity.

The influence of many parameters still remains to be investigated, e.g. perimeters, variable temperature and printing speed or extrusion width. There also seems to be lack of experiments in deformation modes other than uniaxial tension.

Material

The raw material is grey PLA made by the company Filament-PM. The printing properties are 200-230 °C nozzle temperature and 20-60 °C bed temperature. The mechanical properties given by the technical datasheet are: impact strength 16 kJ/m^2 (ISO 179), and flexural modulus 3500 MPa (ISO 178).

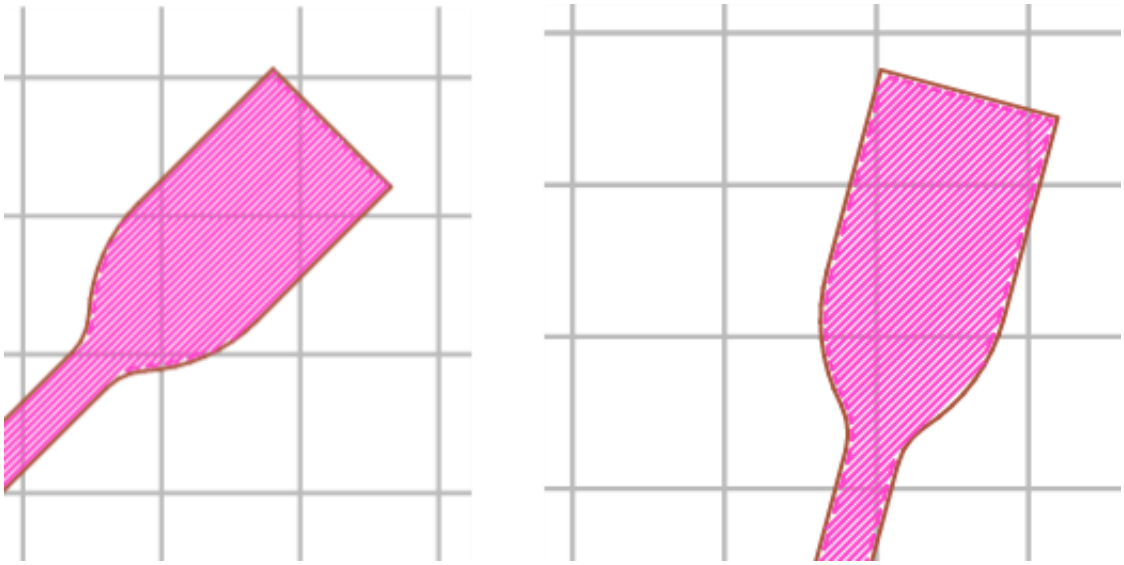

Figure 1. Infills with different orientation angles; 0° left, 30° right

Tensile tests

The outer shape of test specimens was dogbone, type 5A by the standard ČSN EN ISO 527-2 [14]. The instructions for the printer (g-code) were automatically generated using the Slic3r Prusa Edition 1.40.0 with the default settings for the particular material and the Prusa i3 MK3 printer that was used. The most important parameters were:

- layer height 0.15 mm (first layer 0.20 mm),
- nozzle temperature 210 °C (first layer 215 °C),
- bed temperature 60 °C,

- infill density 100 %,
- nozzle diameter 0.4 mm,
- default extrusion width 0.45 mm.

The specimens were labeled according to infill orientation: 0, 30, 60, 90 (angle between the specimen axis and extrusion path - see Figure 1). Specimens of the same infill orientation were distinguished by sequential numbers.

The tests were performed on an electromechanical universal testing machine Zwick/Roell Z050 using a 50 kN load cell. Mechanical extensometer was used to measure strain in the thin middle region. The initial distance of its arms was 15 mm. Monotonic displacement was prescribed with the speed of the clamp of the machine being 2 mm/min in the case of specimen 0/90_01 and 1 mm/min otherwise. All tests were performed at the room temperature, 23±2 °C. Tests 30_02 and 60_01 have been removed from the data due to apparent extensometer slip.

The stress-strain curves in Figure 2 show that the lowest ultimate strength was measured with the 90° infill orientation (43 MPa), the 0° infill exhibits higher ultimate strength (48.0 MPa), and 30° and 60° orientations seem to be even a little stronger (48.8 MPa and 51.3 MPa, respectively). Because the fracture occurred out of the central area in most specimens, see Figure 3, no conclusions were made regarding ultimate strain.

Stiffness was evaluated according to ČSN EN ISO 527-2 [11], Table 1 shows the mean values. The fact that 0° orientation exhibits lower stiffness than 90° is slightly surprising. The reason might lie in the low number of test specimens used for each orientation.

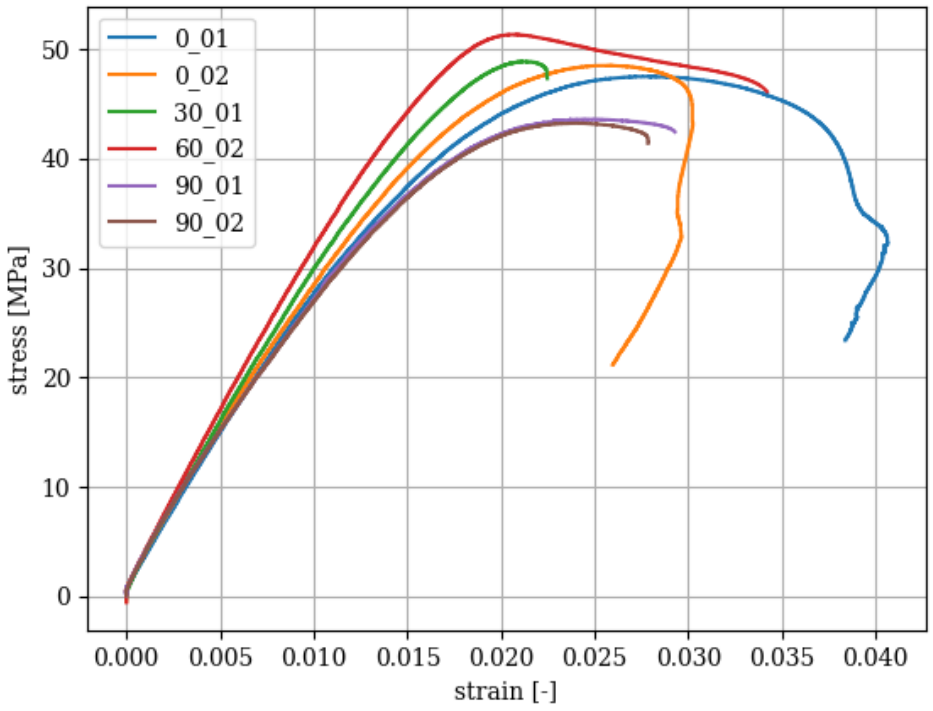

Figure 2. Stress-strain curves.

Table 1: Values of Young's moduli at different infill orientations

Infill angle [°]	0	30	60	90
Young's modulus [GPa]	2.967	3.127	3.287	3.052

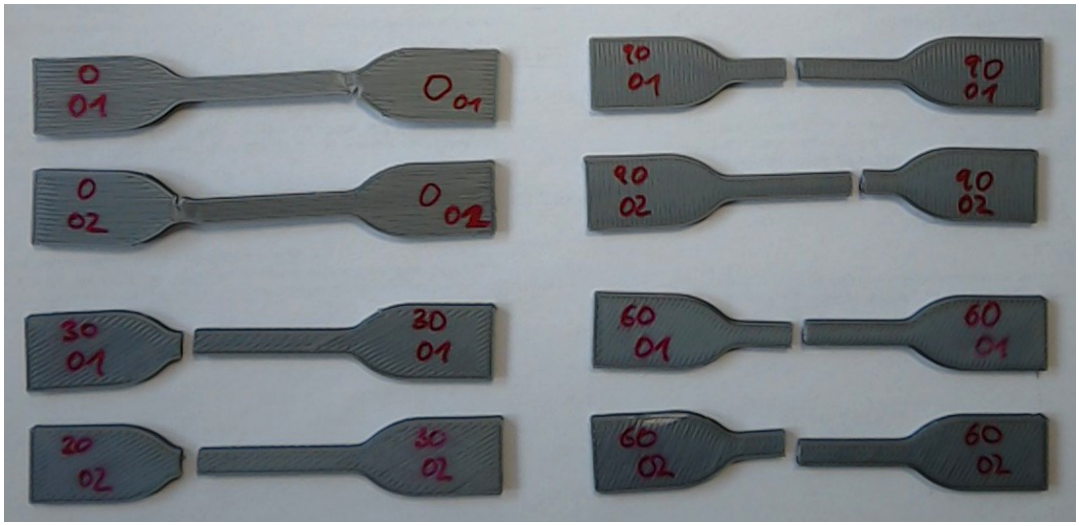

Figure 3. Tensile specimens after the tests.

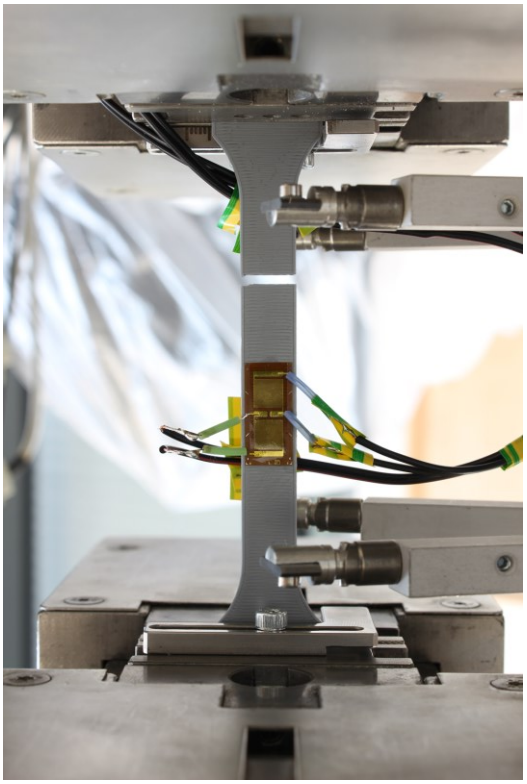

Figure 4. Tensile test with a strain gauge to measure the Poisson's ratio.

Poisson's ratio

Specimens for the evaluation of Poisson's ratio were type 1A by the standard ČSN EN ISO 527-2 [11]. They were printed with the same settings as the tensile specimens. Strain gauges were used to measure strain in the axial (0°) and transverse (90°) directions, see Figure 4. The following values of Poisson's ratios were determined: $\nu_{xy} = 0.3289$, $\nu_{yx} = 0.3267$. These seem to lie within the margin of error.

Material model

Linear material model is considered here, i.e. it obeys the Hooke's law

$$\sigma_{ij} = D_{ijkl}\varepsilon_{kl}. \tag{1}$$

An orthotropic model was considered in plane stress conditions. This leads to the following stress-strain relationship (using the more compact Voigt notation)

$$\begin{bmatrix}\sigma_{xx}\\ \sigma_{yy}\\ \sigma_{xy}\end{bmatrix} = \frac{1}{1-\nu_{xy}\nu_{yx}}\begin{bmatrix}E_x & \nu_{yx}E_x & 0\\ \nu_{xy}E_y & E_y & 0\\ 0 & 0 & G_{xy}(1-\nu_{xy}\nu_{yx})\end{bmatrix}\begin{bmatrix}\varepsilon_{xx}\\ \varepsilon_{yy}\\ 2\varepsilon_{xy}\end{bmatrix}, \tag{2}$$

where the components of the stiffness tensor D^0_{mnpq} transform in the usual way as

$$D^1_{ijkl} = Q_{im}Q_{jn}Q_{kp}Q_{lq}D^0_{mnpq}, \tag{3}$$

Q being the rotation matrix that has the following form

$$Q = \begin{bmatrix}\cos(\alpha) & -\sin(\alpha) & 0\\ \sin(\alpha) & \cos(\alpha) & 0\\ 0 & 0 & 1\end{bmatrix}, \tag{4}$$

upon rotating the specimen infill by the angle α about the z-axis. The Young's modulus in the direction of loading E is computed using the uniaxial relation

$$F = A_0 E\varepsilon_{11} = A_0\sigma_{11} = A_0 D^1_{11kl}\varepsilon_{kl}, \tag{5}$$

where the transversal strain is computed from the condition

$$\sigma_{22} = D^1_{22kl}\varepsilon_{kl} = D^1_{2211}\varepsilon_{11} + D^1_{2222}\varepsilon_{22} = 0 \tag{6}$$

as

$$\varepsilon_{22} = \frac{-D^1_{2211}\varepsilon_{11}}{D^1_{2222}}. \tag{7}$$

Thus, the Young's modulus is

$$E = \frac{F}{A_0\varepsilon_{11}} = D^1_{1111} + D^1_{1122}\frac{\varepsilon_{22}}{\varepsilon_{11}} = D^1_{1111} - D^1_{1122}\frac{D^1_{2211}}{D^1_{2222}}. \tag{8}$$

This relation is, in general, not linear with respect to the material parameters E_x, E_y, ν_{xy}, ν_{yx}, and G_{xy}.

Simple shear test was suggested to overcome non-uniqueness of the calibration process. In this case, the components of strain are $\varepsilon = [0, 0, 2\varepsilon_{12}]^{\mathrm{T}}$ and the stress-strain relationship reduces to $\sigma_{12} = 2D_{1212}\varepsilon_{12}$ with the other stress components being zero.

Calibration

The calibration problem is to find the parameters $\bar{x}$ of the model that minimize a suitable objective function:

$$\bar{x} = \underset{x}{\operatorname{argmin}} f(x). \tag{9}$$

The objective function was chosen in the form of sum of squares of residuals

$$\mathrm{f}(x) = \sum_i (E_i(x) - \bar{E}_i)^2, \tag{10}$$

where $E_i(x)$ is the Young's modulus as computed by the material model (8), $\bar{E}_i$ is the corresponding measured value (see Table 1), and different infill angles are denoted by the index $i \in \{0{,}30°, 60°, 90°\}$. The Levenberg-Marquardt method (see e.g. [15]) was used to solve problem (9)-(10).

As expected, the solution to the calibration problem is not unique with respect to the Poisson's ratios ν_{xy} and ν_{yx}. Therefore, their values were measured using the strain gauges and fixed. Thus, only three optimization parameters remained, $x = [E_x, E_y, G_{xy}]$. The resulting values are shown in Table 2. History of the objective function and optimization parameters is shown in Figure 5 and 6, respectively. The data (Young's moduli) are compared to the prediction of the calibrated model in Figure 7.

Table 2: Calibration results

E_x [GPa]	E_y [GPa]	G_{xy} [GPa]
2.943	3.075	1.288

The following procedure was employed in order to quantify the limits of use of the calibrated material (see Figure 8). Upper and lower bounds of stress were chosen for each infill angle as:

$$\sigma_{\text{upper}}(\varepsilon) = 1.05 \max_i \{\sigma_i(\varepsilon)\}, \tag{11}$$

$$\sigma_{\text{lower}}(\varepsilon) = 0.95 \min_i \{\sigma_i(\varepsilon)\}, \tag{12}$$

where $\sigma_i(\varepsilon)$ denotes the stress-strain curves determined experimentally. The model is considered usable at strain ε if the stress predicted by the model, $\sigma(\varepsilon)$, lies between the upper and lower bound

$$\sigma_{\text{lower}}(\varepsilon) \leq \sigma(\varepsilon) \leq \sigma_{\text{upper}}(\varepsilon). \tag{13}$$

Table 3 shows the limit strains beyond which the above relation no longer holds.

Table 3: Limits of use of the calibrated model in terms of tensile strain

Infill angle [°]	0	30	60	90
Strain limit of use [%]	0.91	0.79	1.06	0.47

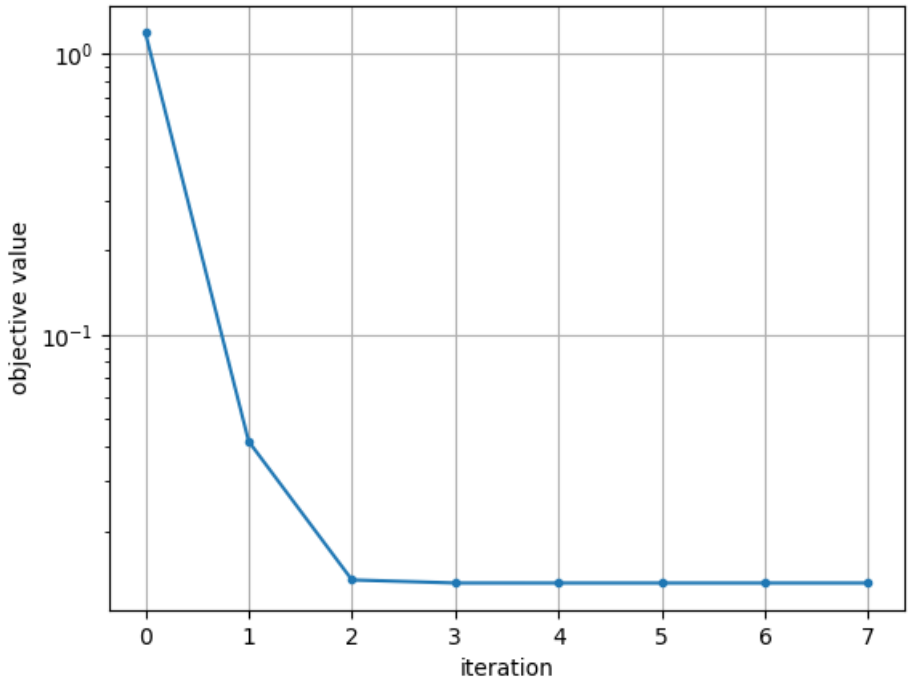

Figure 5. History of the objective function.

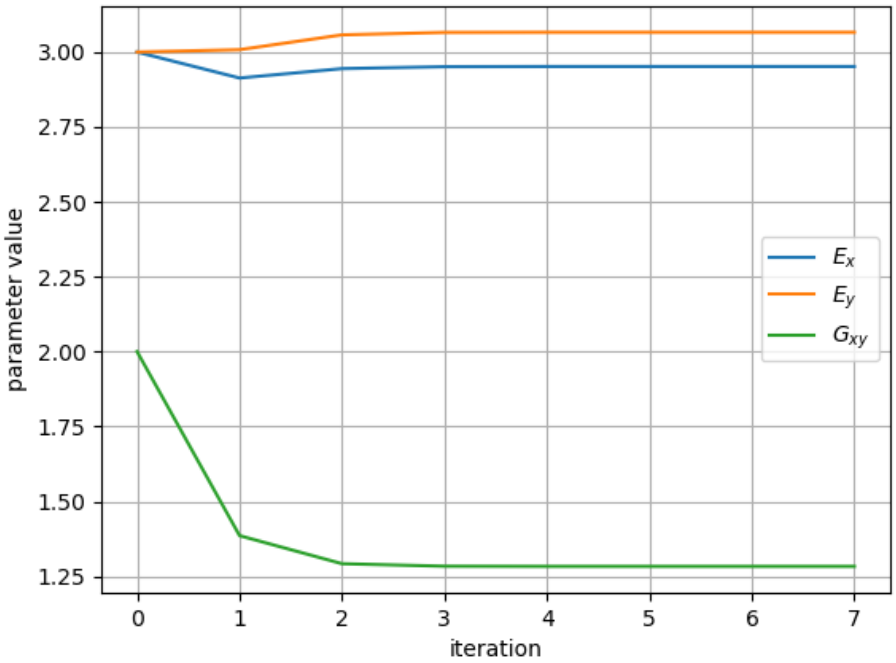

Figure 6. History of the optimization parameters.

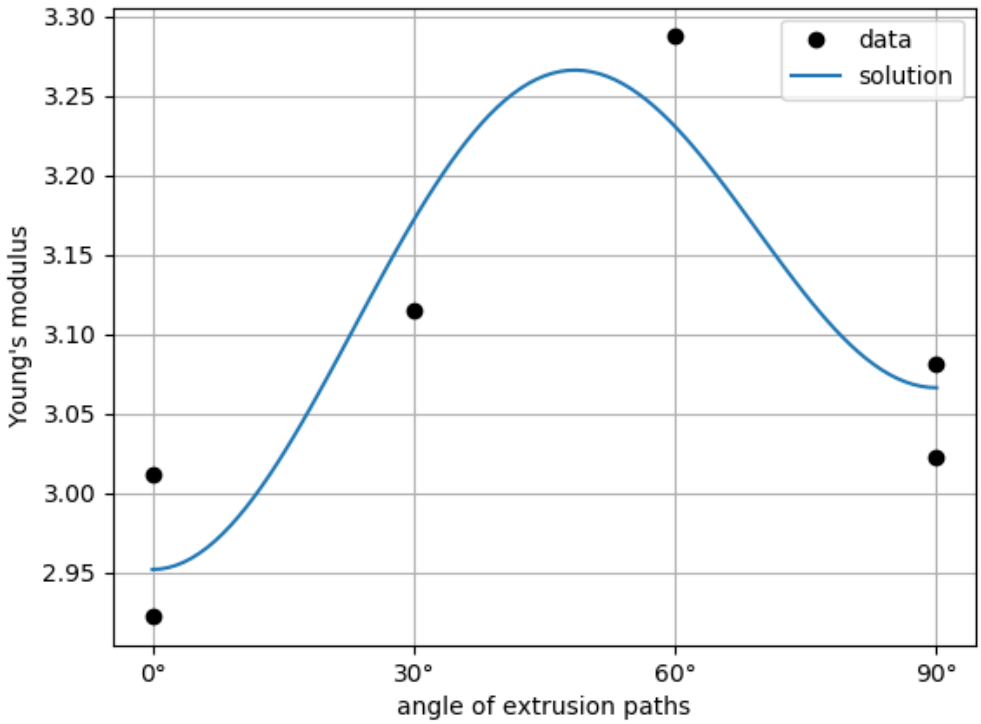

Figure 7. Data (Young's moduli for different infill angles) and the calibrated model.

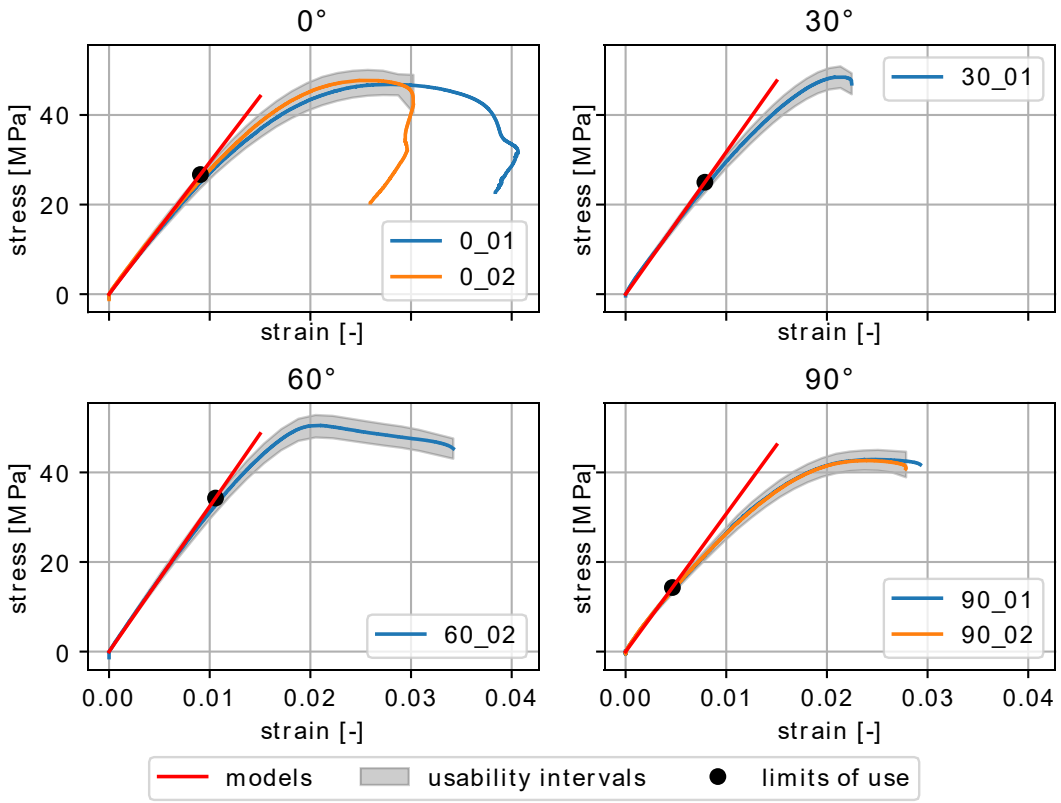

Figure 8. Limits of use of the calibrated model. The grey areas represent the intervals inside which the model is considered to describe the data accurately enough. The black dots mark the points at which the model exits these intervals.

Conclusions

Contrary to the expectation, stiffness in the direction of the extruded paths (0° angle) is lower than in the perpendicular direction (90°), while the opposite holds for ultimate strength. The directions in between (30° and 60°) exhibit higher stiffness.

The linear orthotropic model is capable of modeling the material for reasonably small strains. Successful calibration of this model requires knowledge of Poisson's ratios and tensile tests in other than the principal directions or a shear test, since the shear modulus, G_{xy}, strongly affect the stiffness in rotated coordinates.

Acknowledgement

This publication was supported by the project LO1506 of the Czech Ministry of Education, Youth and Sports under the program NPU I.

References

[1] A. Derossi, M. Paolillo, R. Caporizzi, C. Severini, Extending the 3D food printing tests at high speed. Material deposition and effect of non-printing movements on the final quality of printed structures, Journal of Food Engineering 275 (2020) Art. No. 109865.

[2] E. Saygilia, A. A. Dogan-Gurbuzb, O. Yesil-Celiktasa, M.S. Draz, Review article3D bioprinting: A powerful tool to leverage tissue engineering andmicrobial systems, Bioprinting 18 (2020) Art. No. e00071.

[3] X. Kuang, D. J. Roach, J. Wu, C. M. Hamel, Z. Ding, T. Wang, M. L. Dunn, H. J. Qi, Advances in 4D Printing: Materials and Applications, Adv. Funct. Mater. 29 (2019), Art. No. 1805290.

[4] A.C. Abbott, G.P. Tandona, R.L. Bradford, H. Koerner, J.W. Baur, Process-structure-property effects on ABS bond strength in fused filament fabrication, Additive Manufacturing 19 (2018) 29-38.

[5] B.M. Tymrak, M. Kreiger, J.M. Pearce, Mechanical properties of components fabricated with open-source 3-D printers under realistic environmental conditions, Materials and Design 58 (2014) 242-246.

[6] P. Ramkumar, Investigation on the Effect of Process Parameters on Impact Strength of Fused Deposition Modelling Specimens, in: IOP Conf. Series: Materials Science and Engineering 491 (2019) Art. No. 012026.

[7] A. Andrzejewska, Ł. Pejkowski, T. Topoliński, Tensile and Fatigue Behavior of Additive Manufactured Polylactide, 3D Printing and Additive Manufacturing, Vol. 6, No. 5 (2019) 272-280.

[8] M. Fernandez-Vicente, W. Calle, S. Ferrandiz, A. Conejero, Effect of Infill Parameters on Tensile Mechanical Behavior in Desktop 3D Printing, 3D Printing and Additive Manufacturing, Vol. 3, No. 3 (2016), 183-192.

[9] J. Nomania, D. Wilsonb, M. Paulinob, M. I. Mohammed, Effect of layer thickness and cross-section geometry on the tensile and compression properties of 3D printed ABS, Materials Today Communications 22 (2020) Art. No. 100626.

[10] A. Pandzic, D. Hodzic, A. Milovanovic, Influence of Material Colour on Mechanical Properties of PLA Material in FDM Technology, in: Proceedings of the 30th DAAAM International Symposium, Vienna, Austria, 2019, pp. 0555-0561.

[11] W. M. H. Verbeetena, M. Lorenzo-Bañuelosa, P. J. Arribas-Subiñas, Anisotropic rate-dependent mechanical behavior of Poly(Lactic Acid) processed by Material Extrusion Additive Manufacturing, Additive Manufacturing 31 (2020) Art. No. 100968.

[12] P. Doungkom, K. Jiamjiroch, Analysis of Printing Pattern and Infiltration Percent over the Tensile Properties of PLA Printed Parts by a Fuse Deposition Modelling Printer, IOP Conf. Series: Materials Science and Engineering 501 (2019) 012028.

[13] C.-Y. Lee, C.-Y. Liu, The influence of forced-air cooling on a 3D printed PLA part manufactured by fused filament fabrication, Additive Manufacturing 25 (2019) 196-203.

[14] ČSN EN ISO 527-2 (2012) Plastics - Determination of tensile properties - Part 2: Test conditions for moulding and extrusion plastics.

[15] W. H. Press, S. A. Teukolsky, W. T. Vetterling, B. P. Flannery, Numerical Recipes in C, second ed., Cambridge University Press, Cambridge, 1992.